

# RSC Advances



This is an *Accepted Manuscript*, which has been through the Royal Society of Chemistry peer review process and has been accepted for publication.

*Accepted Manuscripts* are published online shortly after acceptance, before technical editing, formatting and proof reading. Using this free service, authors can make their results available to the community, in citable form, before we publish the edited article. This *Accepted Manuscript* will be replaced by the edited, formatted and paginated article as soon as this is available.

You can find more information about *Accepted Manuscripts* in the [Information for Authors](#).

Please note that technical editing may introduce minor changes to the text and/or graphics, which may alter content. The journal's standard [Terms & Conditions](#) and the [Ethical guidelines](#) still apply. In no event shall the Royal Society of Chemistry be held responsible for any errors or omissions in this *Accepted Manuscript* or any consequences arising from the use of any information it contains.

---

## Shape-Dependent Photocatalytic Activity of Bi<sub>5</sub>O<sub>7</sub>I Caused by Facets Synergetic and Internal Electric Field Effects

Yurong Su,<sup>a</sup> Hui Wang,<sup>b</sup> Liqun Ye,<sup>a\*</sup> Xiaoli Jin,<sup>a</sup> Haiquan Xie,<sup>a\*</sup> Chaozheng He<sup>c</sup> and Keyan Bao<sup>a</sup>

<sup>a</sup> College of Chemistry and Pharmaceutical Engineering, Nanyang Normal University, Nanyang 473061, People's Republic of China.

<sup>b</sup> CAS Key Laboratory of Nuclear Radiation and Nuclear Energy Techniques, and Multidisciplinary Initiative Center, Institute of High Energy Physics, Chinese Academy of Sciences, Beijing, 100049, China.

<sup>c</sup> College of Physics and Electronic Engineering, Nanyang Normal University, Nanyang 473061, People's Republic of China.

### Corresponding Author

\* E-mail: yeliquny@163.com (L. Ye)

Xie-hq@163.com (H. Xie)

**KEYWORDS:** Bi<sub>5</sub>O<sub>7</sub>I; shape; photocatalysis; internal electric field; facet synergetic

---

**ABSTRACT:** Bi<sub>5</sub>O<sub>7</sub>I rods and Bi<sub>5</sub>O<sub>7</sub>I sheets photocatalytic materials were synthesized by hydrothermal method and solid phase conversion, respectively. They were characterized by X-ray diffraction patterns (XRD), selected area electron diffraction (SAED), field emission scanning electron microscope (FESEM), high-resolution transmission electron microscopy (HRTEM) and UV-vis diffuse reflectance spectra (DRS). The photocatalytic results showed that Bi<sub>5</sub>O<sub>7</sub>I had shape-dependent photocatalytic activity. Bi<sub>5</sub>O<sub>7</sub>I rods showed much higher photocatalytic activity than Bi<sub>5</sub>O<sub>7</sub>I sheets for the degradation of dyes. Photoluminescence (PL) spectra, active species trapping and theoretical calculation were studied to analyze the photocatalytic mechanisms of the shape-dependent photocatalytic activity. It revealed that Bi<sub>5</sub>O<sub>7</sub>I rods with {001} and {100} facets exposure result in synergetic and internal electric field effects. So, higher separation efficiency of photogenerated carriers and photocatalytic activity were revealed for Bi<sub>5</sub>O<sub>7</sub>I rods.

---

## 1 Introduction

With the huge consumption of traditional fossil fuels for urbanization and industrialization in the past several years, human confront great energy crisis and environmental pollution issues.<sup>1-3</sup> Photoenergy was suggested as an efficient, green energy to solve the energy crisis and environmental decontamination with light-capture nanomaterials using.<sup>4-5</sup> For example, titanium dioxide (TiO<sub>2</sub>), the most classical photocatalyst, have been widely used for water splitting into H<sub>2</sub> gas,<sup>6</sup> harmful pollutants decomposition,<sup>2</sup> and CO<sub>2</sub> conversion to energy bearing carbon fuel sources.<sup>7</sup> However, all researchers know that TiO<sub>2</sub> can not utilize visible light due to its wide band-gap of 3.2 eV. In order to enhance the utilization efficiency of photoenergy, many new photocatalysts were studied, such as AgX (X = Cl, Br),<sup>8-10</sup> AgPO<sub>4</sub>,<sup>11,12</sup> graphitic-C<sub>3</sub>N<sub>4</sub>,<sup>13,14</sup> red phosphorus,<sup>15</sup> and  $\alpha$ -sulfur.<sup>16</sup> But, these photocatalysts also face many new problems, such as photo-stabilization of Ag-based photocatalysts,<sup>8-12</sup> and low quantum yields of polymer or element semiconductor photocatalysts.<sup>13-16</sup>

Recently, BiOX (X = Cl, Br, I) photocatalysts were proved that they have very high photocatalytic activity for harmful pollutants decomposition.<sup>3,17,18</sup> In previous works, the origin of high photocatalytic activity has been summarized and suggested as the layered structure which displays high internal electric field.<sup>19,20</sup> However, BiOX photocatalysts also have an obvious shortcoming. The conduction band minimum (CBM) of BiOX photocatalysts are very positive.<sup>21-23</sup> So, the photocatalytic reduction activity of BiOX is very low. And it also results in the weak photocatalytic activity for pollutants decomposition. Among BiOX photocatalysts, BiOI has the most positive CBM. To enhance its photocatalytic activity, the CBM must be decreased. Theoretical calculation showed that the CBM of bismuth-based compound mainly consists of Bi 6p orbits.<sup>19</sup> Therefore, the content of bismuth may decrease the CBM potential, and then, the bismuth-rich bismuth oxyhalide photocatalysts showed very high photocatalytic reduction activity.<sup>24-26</sup> For instances, by bismuth-rich strategy, Bi<sub>24</sub>O<sub>31</sub>Br<sub>10</sub> can photocatalytic reduce Cr (VI) and split water,<sup>24</sup> and Bi<sub>3</sub>O<sub>4</sub>Br can effectively activate molecular oxygen.<sup>26</sup> In this work, via bismuth-rich strategy, Bi<sub>5</sub>O<sub>7</sub>I samples were synthesized, and their photocatalytic activities also were studied.

In general, different shape of semiconducting photocatalyst has different facets exposure. And the different crystal facets display different atomic arrangement and electronic structure. So, the photocatalyst with different shape may reveal different photocatalytic activity. For examples, the shape-dependent photocatalytic activity of TiO<sub>2</sub>,<sup>27,28</sup> Cu<sub>2</sub>O,<sup>29</sup> AgBr,<sup>30</sup> AgPO<sub>4</sub>,<sup>31</sup> BiVO<sub>4</sub><sup>32</sup> were suggested by facet effects. Here, Bi<sub>5</sub>O<sub>7</sub>I rods and Bi<sub>5</sub>O<sub>7</sub>I sheets were synthesized, and they showed shape-dependent

photocatalytic activity. The photocatalytic mechanism studies indicated that the origin caused by facets synergetic and internal electric field effects.

## 2 Experimental

### 2.1 Materials

$\text{Bi}(\text{NO}_3)_3 \cdot 5\text{H}_2\text{O}$ , KI, p-benzoquinone (BQ), triethanolamine (TEOA), isopropanol (IPA),  $\text{AgNO}_3$  and ethanol were analytical pure and from Sinopharm Chemical Reagent Co., Ltd. Rhodamine B (RhB) and methyl orange (MO) were analytical pure and used without further purification.

### 2.2 Synthesis

**BiOI:** In this work, the precursors for preparing  $\text{Bi}_5\text{O}_7\text{I}$  sheets and rods are BiOI. And the BiOI precursor was synthesized via a chemical precipitation method as follows: 10 mL KI (1 mol/L) solution was added into the 200 mL  $\text{Bi}(\text{NO}_3)_3 \cdot 5\text{H}_2\text{O}$  (0.05 mol/L) solution drop by drop with continuously stirring for 12 h at 60 °C. And then, red precipitate was obtained. After, BiOI precursor was collected, washed with absolute ethanol and deionized water three times and transferred to an oven to dry at 80 °C in air.

**$\text{Bi}_5\text{O}_7\text{I}$  rods:** 1.0 g BiOI precursor was dispersed in 30 mL deionized water. Then 1 mol/L NaOH solution was used to adjust the pH value of the above dispersion to 13 with magnetic stirring. After stirring 1 h, the suspension was transferred into Teflon-lined stainless steel autoclaves (50 mL), and then the autoclaves were kept at 160 °C for 24 h. After reaction, the yellow  $\text{Bi}_5\text{O}_7\text{I}$  rods precipitate was obtained by centrifugation, then washed successively with 0.001 M HCl solution and distilled water until pH = 7.0. Finally, it was dried at 80 °C.

**$\text{Bi}_5\text{O}_7\text{I}$  sheets:** 1.0 g BiOI precursor was calcinated at 350 °C for 3 h. Then yellow  $\text{Bi}_5\text{O}_7\text{I}$  sheets sample was obtained.

### 2.3 Characterization

X-ray diffraction patterns (XRD) of the samples were recorded at room temperature, by a Bruker D8 advance X-ray diffractometer using Cu  $K\alpha$  radiation and  $2\theta$  scan rate of  $6 \text{ min}^{-1}$ . Diffraction patterns were taken over the  $2\theta$  range of 20-80°. FESEM images were obtained by a JEOL JEM-7600F Field Emission Scanning Electron Microscope. Transmission electron microscopy (TEM) and high-resolution transmission electron microscopy (HRTEM) images were obtained by a JEOL JEM-2100 (RH) Field Emission Electron Microscope. UV-vis diffuse reflectance spectra (DRS) were obtained using a Shimadzu UV-3600 spectrometer by using  $\text{BaSO}_4$  as a reference. Photoluminescence (PL) spectra of  $\text{Bi}_5\text{O}_7\text{I}$  samples were obtained by a Cary Eclipse spectro-photometer with  $\lambda_{\text{exc}} = 320 \text{ nm}$ . The Brunauer–Emmett–Teller (BET) surface areas of  $\text{Bi}_5\text{O}_7\text{I}$  samples were measured using quantachrome

autosorb-1 automated gas sorption systems at 77 K. The infrared spectra were obtained on a Nicolet 5700 Fourier transform infrared (FT-IR) spectrometer with KBr as the reference sample within a wavelength range of 400–4000  $\text{cm}^{-1}$ .

## 2.4 Photocatalytic activity test

The photocatalytic activities were evaluated by the degradation of RhB under a 500 W high pressure xenon lamp (Changzhou Yuyu Electro-Optical Device Co., Ltd. China). Typical photocatalytic degradation process is arranged in this way: 100 mL aqueous suspension of 11 mg/L RhB was placed in a glass beaker, and then 20 mg photocatalysts were added. Prior to irradiation, the suspension was sonicated for 10 min and then magnetically stirred in dark for 30 min to get desorption-adsorption equilibrium. The suspension was kept under constant air-equilibrated conditions during irradiation. A magnetic stirrer was employed for continuous mixing. At certain time intervals, 4 mL suspensions were sampled and centrifuged by TGL-16G centrifuge (Shanghai Anting Scientific Instrument Factory, China) at 10 000 rpm for 15 min to remove the particles. The upper clear liquid was analyzed by recording the maximum absorption band (554 nm for RhB) using a 721 spectrophotometer (Shanghai yoke, China).

## 2.5 Active species trapping

For detecting the active species during photocatalytic reactivity, hydroxyl radicals ( $\bullet\text{OH}$ ), superoxide radical ( $\text{O}_2^{\bullet-}$ ), electron ( $\text{e}^-$ ) and holes ( $\text{h}^+$ ) were investigated by adding 1.0 mM IPA (a quencher of  $\bullet\text{OH}$ ), BQ (a quencher of  $\text{O}_2^{\bullet-}$ )  $\text{AgNO}_3$  and TEOA (a quencher of  $\text{h}^+$ ), respectively.<sup>21-23</sup>

## 2.6 Theoretical calculation method

First-principles studies were carried out using plane-wave method as implemented in the Vienna ab initio simulation package (VASP).<sup>33,34</sup> The Perdew-Burke-Ernzerhof (PBE) function with the generalized gradient approximation (GGA) was used to describe the ion-electron interaction and the core electrons were described by the full-potential projector augmented wave (PAW) method with an energy cutoff of 500 eV for the plane-wave expansion.<sup>35-37</sup> Geometry optimization was performed using the conjugate gradient algorithm until the force on each atom was less than 0.03 eV/Å, and the spin polarization was considered. Integrations in the Brillouin zone were performed using k-point grid generated with the Monkhorst–Pack grid.

# 3 Results and discussion

## 3.1 Catalyst characterization

Fig. 1 showed the XRD patterns of  $\text{Bi}_5\text{O}_7\text{I}$  rods and  $\text{Bi}_5\text{O}_7\text{I}$  sheets. All XRD peaks of  $\text{Bi}_5\text{O}_7\text{I}$  rods and  $\text{Bi}_5\text{O}_7\text{I}$  sheets can be indexed to the orthorhombic  $\text{Bi}_5\text{O}_7\text{I}$  (JCPDS file No. 40-0548). It can be found that there are three peaks (312), (004) and (020) at  $2\theta$  of 28.08°, 31.09° and 33.43°, respectively. In addition,

no other characteristic peaks of impurity (such as BiOI and Bi<sub>2</sub>O<sub>3</sub>) were detected in the above two samples. It indicates that Bi<sub>5</sub>O<sub>7</sub>I rods and Bi<sub>5</sub>O<sub>7</sub>I sheets samples are all pure Bi<sub>5</sub>O<sub>7</sub>I.

<Inset Fig. 1>

In order to obtain the morphology and exposed facets of Bi<sub>5</sub>O<sub>7</sub>I rods and Bi<sub>5</sub>O<sub>7</sub>I sheets, the FESEM, SAED, HRTEM and FFT analysis have been done (Fig. 2). For Bi<sub>5</sub>O<sub>7</sub>I sheets sample, it has a size of about 1.5 μm × 1.5 μm and thickness of about 0.3 μm. Although Bi<sub>5</sub>O<sub>7</sub>I sheets have been reported in some works, the exposed facets have not reported until now. Fig. 2b showed the SAED pattern of Bi<sub>5</sub>O<sub>7</sub>I sheets. It displayed diffraction spots of (312), (31-2) and (004). And angles of (312)-(31-2) and (004)-(312) were 67.6 and 56.4°, respectively, which are consistent with the theoretical interfacial angles between {312} and {31-2} facets (67.1°) and between {312} and {004} facets (56.5°). They proved that the main exposed facets of Bi<sub>5</sub>O<sub>7</sub>I sheets are (1-30) facets. It can be found that the main exposed facets of Bi<sub>5</sub>O<sub>7</sub>I sheets are different with the reported exposed facets of BiOI ({001} or {100} facets), although Bi<sub>5</sub>O<sub>7</sub>I and BiOI are inorganic graphene materials. For checking our result again, the HRTEM and the corresponding FFT pattern were showed in Fig. 3c. The distinct lattice fringe of d = 0.286 nm matches with the crystallographic plane of Bi<sub>5</sub>O<sub>7</sub>I (004). The inset picture of Fig. 2c display that the angles of (312)-(31-2) and (004)-(312) were 67.3 and 56.0°, which also are consistent with the theoretical interfacial angles. So, we can conclude that the main exposed facet of Bi<sub>5</sub>O<sub>7</sub>I sheets is {1-30} facet.

<Inset Fig. 2>

<Inset Fig. 3>

For Bi<sub>5</sub>O<sub>7</sub>I rods sample, the length was about 10 μm and the width was about 0.5 μm as shown in Fig. 2d. Fig. 3e showed the SAED pattern of Bi<sub>5</sub>O<sub>7</sub>I rods. It displayed diffraction spots of (004), (020) and (024). And angles of (004)-(024) and (020)-(024) were 46.8 and 42.8°, which are consistent with the theoretical interfacial angles between {004} and {024} facets (47.0°) and between {020} and {024} facets (43.0°). In addition, the HRTEM and the corresponding FFT pattern of Bi<sub>5</sub>O<sub>7</sub>I rods were showed in Fig. 3f. The distinct lattice fringes of d = 0.573 nm and 0.528 nm, match with the crystallographic plane of Bi<sub>5</sub>O<sub>7</sub>I (002) and (010), respectively. And the angle between of (002) and (010) was 89.5°, which is consistent with the theoretical interfacial angle (90.0°). The inset picture of Fig. 3c displayed that the angles of (004)-(024) and (020)-(024) are 46.6 and 43.8°, which also are consistent with the theoretical interfacial angle. They proved that the main exposed facets of Bi<sub>5</sub>O<sub>7</sub>I sheets are (001) and {100} facets, and our result is in accord with reported result.

The comparison of UV-vis diffuse reflectance spectra (DRS) of Bi<sub>5</sub>O<sub>7</sub>I rods and Bi<sub>5</sub>O<sub>7</sub>I sheets were shown in Fig. 3a. Both Bi<sub>5</sub>O<sub>7</sub>I samples showed a strong absorption under visible range. And the

absorption edge of Bi<sub>5</sub>O<sub>7</sub>I rods and Bi<sub>5</sub>O<sub>7</sub>I sheets were 506 nm and 523 nm, respectively. Because Bi<sub>5</sub>O<sub>7</sub>I is indirect excitation photocatalyst, the band gap energy ( $E_g$ ) were calculated from the plot of  $(\alpha h\nu)^{1/2}$  versus energy ( $h\nu$ ) as shown in Fig.3b.<sup>18</sup> The  $E_g$  of Bi<sub>5</sub>O<sub>7</sub>I rods and Bi<sub>5</sub>O<sub>7</sub>I sheets were 2.39 eV and 2.47 eV, respectively. Clearly, Bi<sub>5</sub>O<sub>7</sub>I sheets can absorb more visible light, but Bi<sub>5</sub>O<sub>7</sub>I rods displayed higher band gap energy.

### 3.2 Photocatalytic activity

At present, the most application of Bi-O-X (X = Cl, Br, I) series photocatalytic materials was used to degrade dyes. Here, RhB (cationic dye) and MO (anionic dye) were used as a model pollutant to study the photocatalytic activity of Bi<sub>5</sub>O<sub>7</sub>I samples. Fig. 4a showed the photocatalytic degradation experiment result of RhB by Bi<sub>5</sub>O<sub>7</sub>I rods and Bi<sub>5</sub>O<sub>7</sub>I sheets. It can be found that, under Xe lamp irradiation, RhB self-photolysis degradation without Bi<sub>5</sub>O<sub>7</sub>I photocatalyst was not observable, which indicated that RhB is stable under Xe lamp irradiation. After 80 min Xe lamp irradiation, RhB removal over Bi<sub>5</sub>O<sub>7</sub>I sheets is as low as 17%. Significantly, the photocatalytic activity of Bi<sub>5</sub>O<sub>7</sub>I rods displayed intensively increases, which induced 85% degradation within 80 min. This result indicated that Bi<sub>5</sub>O<sub>7</sub>I rods display much better photocatalytic activity than that of Bi<sub>5</sub>O<sub>7</sub>I sheets.

#### <Inset Fig. 4>

It is generally known that Bi-O-X (X = Cl, Br, I) series photocatalytic materials may shown photocatalytic selectivity for dyes degradation due to their electronegativity of exposed facets. For example, in our previous work, it was proved that BiOI can photocatalytic remove cationic dye more efficiently than anionic dye due to the {001} facet exposure.<sup>23</sup> So, cationic dye and anionic dye should be used simultaneously to prove the photocatalytic activity of Bi<sub>5</sub>O<sub>7</sub>I samples with different shapes. As shown in Fig. 4b, the photocatalytic result for anionic dye MO degradation was same with cationic dye RhB. Therefore, we can conclude that Bi<sub>5</sub>O<sub>7</sub>I rods display much better photocatalytic activity than that of Bi<sub>5</sub>O<sub>7</sub>I sheets.

### 3.3 Photocatalytic mechanism

The photocatalytic performances of pure photocatalytic materials are mainly affected by specific surface area and phase composition.<sup>1,6</sup> Recently, the shape and exposed facets of photocatalytic materials have been proved to be very important factors influencing the photocatalytic activity. In this work, Bi<sub>5</sub>O<sub>7</sub>I rods and Bi<sub>5</sub>O<sub>7</sub>I sheets had same phase composition (orthorhombic Bi<sub>5</sub>O<sub>7</sub>I) and approximately specific surface area (1.4 m<sup>2</sup>/g for Bi<sub>5</sub>O<sub>7</sub>I rods and 1.2 m<sup>2</sup>/g for Bi<sub>5</sub>O<sub>7</sub>I sheets) and same surface characteristics (Fig. S1). So, the shape-dependent photocatalytic activity of Bi<sub>5</sub>O<sub>7</sub>I may be caused by shape effect and facet effect.

In very recently reports, it has been proved that shape and facet can affect the surface atomic arrangement and electronic structure, which can result in the difference on separation efficiency of photogenerated carriers. And then, the photocatalytic materials with different shapes and exposed facets may show different photocatalytic activity.<sup>27-32</sup> In order to compare the separation efficiency of photogenerated carriers, PL spectra of Bi<sub>5</sub>O<sub>7</sub>I sheets and Bi<sub>5</sub>O<sub>7</sub>I rods were done. PL spectra have been often employed to study separation efficiency of photogenerated carriers of photocatalytic materials. With photogenerated carriers recombination after a photocatalyst was irradiated, photons are emitted, resulting in photoluminescence. Fig. 5 showed a comparison of the PL spectra between Bi<sub>5</sub>O<sub>7</sub>I rods and Bi<sub>5</sub>O<sub>7</sub>I sheets under the excitation at 320 nm. The PL spectrum for Both Bi<sub>5</sub>O<sub>7</sub>I samples were characterized by a peak at 498 nm, which attributed to the emission of band gap transition energy of Bi<sub>5</sub>O<sub>7</sub>I samples (506 nm for Bi<sub>5</sub>O<sub>7</sub>I sheets and 523 for Bi<sub>5</sub>O<sub>7</sub>I rods). In addition, the fluorescence intensity of Bi<sub>5</sub>O<sub>7</sub>I rods is smaller than that of Bi<sub>5</sub>O<sub>7</sub>I sheets. It indicated that the rods shape can be beneficial to the separation of electron-hole pairs under irradiation.

<Inset Fig. 5>

As far as we know, the internal electric field strongly influences the separation efficiency of photogenerated carriers of Bi-O-X series photocatalytic materials.<sup>38,39</sup> For Bi<sub>5</sub>O<sub>7</sub>I, the internal static electric fields along with the [001] orientation and enhanced the effective separation of the photoinduced carriers (Fig. S2). As schematically illustrated in Scheme 1, the internal electric field is perpendicular to the Bi<sub>5</sub>O<sub>7</sub>I rods but parallel to those of Bi<sub>5</sub>O<sub>7</sub>I sheets. Therefore, the carriers separation and transfer assisted by the internal electric fields are more favorable in Bi<sub>5</sub>O<sub>7</sub>I rods, as confirmed by PL spectrum.

For further studying the origin of rods shape enhanced separation efficiency photogenerated carriers, First-principles studies were carried out using plane-wave method to evaluate the electronic structures of {100} and {001} facets of Bi<sub>5</sub>O<sub>7</sub>I. As shown in Fig. 6, the band structures of {100} and {001} facets were calculated by VASP. It is clear that the valence band maximum (VBM) mainly consists of O 2p and I 5p orbits, while the conduction band minimum (CBM) mainly consists of Bi 6p orbits. It is in agreement with reported results.<sup>25</sup> On the other hand, it can be seen that the CBM of {100} facets is more positive than that of {001} facets. So, as shown in Scheme 2, the photogenerated electrons can transfer from {001} facets to {100} facets by facets synergetic effect. And then, electrons can be retained more effectively and the separation of electron-hole pairs can be enhanced. So, Bi<sub>5</sub>O<sub>7</sub>I rods with {100} and {001} facets exposure showed higher photocatalytic activity than that of Bi<sub>5</sub>O<sub>7</sub>I sheets.

<Inset Fig. 6>

---

**<Inset Fig. 7>**

On the other hand, we also found that the VBM of {100} and {001} facets are at the same position. It imply that photogenerated holes may not can transfer between {001} facets to {100} facets. And electron can not used to degrade dyes. But, the migration velocity of electron is much higher than hole due to the smaller quality. So, the photogenerated electron transfer is more important than that of holes, and results in more effectively separation of electron-hole pairs and higher photocatalytic activity.

Fig. 7 showed the trapping experiment of active species during the photocatalytic reaction the PCD of RhB was not affected by the addition of AgNO<sub>3</sub> (a quencher of e<sup>-</sup>) and IPA (a quencher of •OH). On the contrary, the PCD of RhB decreased after adding TEOA (a quencher of h<sup>+</sup>) and BQ (a quencher of O<sub>2</sub><sup>•-</sup>). It indicated that the main active species are h<sup>+</sup> and O<sub>2</sub><sup>•-</sup> rather than e<sup>-</sup> or •OH.

**<Inset Scheme. 1>****<Inset Scheme. 2>**

On the base of Fig. 5, 6 and 7, it can be described the photocatalytic mechanism of shape-dependent photocatalytic activity of Bi<sub>5</sub>O<sub>7</sub>I as shown in Scheme 1. Basing on the internal electric field direction, it can be seen that the separation efficiency of photogenerated carriers of Bi<sub>5</sub>O<sub>7</sub>I rods is better than Bi<sub>5</sub>O<sub>7</sub>I sheets. And due to the facets synergetic effect between {100} and {001} facets, under Xe lamp irradiation, photogenerated electrons can transfer from {001} facets to {100} facets. And then, the photogenerated carriers are separated very well. So, Bi<sub>5</sub>O<sub>7</sub>I rods can degrade dyes efficiently. In a word, the shape-dependent photocatalytic activity of Bi<sub>5</sub>O<sub>7</sub>I is aroused by facets synergetic and internal electric field effects.

**4. Conclusions**

In this paper, Bi<sub>5</sub>O<sub>7</sub>I rods and Bi<sub>5</sub>O<sub>7</sub>I sheets were synthesized by hydrothermal method and solid phase conversion, respectively. After comparing the photocatalytic activity of both Bi<sub>5</sub>O<sub>7</sub>I samples, we found that Bi<sub>5</sub>O<sub>7</sub>I display shape-dependent photocatalytic activity. Bi<sub>5</sub>O<sub>7</sub>I rods showed much higher photocatalytic activity than Bi<sub>5</sub>O<sub>7</sub>I sheets for dyes degradation. The date about PL spectra, active species trapping and theoretical calculation indicated that the {001} and {100} facets exposure of Bi<sub>5</sub>O<sub>7</sub>I rods can result in synergetic and internal electric field effects simultaneously. So, Bi<sub>5</sub>O<sub>7</sub>I rods revealed higher photocatalytic activity. This finding in this work may potentially be extended to other Bi-based semiconductor photocatalysts, such as Bi<sub>3</sub>O<sub>4</sub>X (X= Cl, Br) and Bi<sub>24</sub>O<sub>31</sub>X<sub>10</sub> (X= Cl, Br) to find best shape for photocatalysis.

**ACKNOWLEDGMENT**

This work was supported by the Henan Joint Funds of the National Natural Science Foundation of China (No. U1404506, U1404216), Natural Science Foundation of Henan Department of Science & Technology (No. 142102210477), Natural Science Foundation of Henan Department of Education (No. 14A150021), Natural Science Foundation of Nanyang Normal University (No. ZX2014039, ZX2014088), and the Chinese Academy of Sciences in the framework of a Frontier of Novelty program to D. Wang (No. Y2291810S3).

## REFERENCES

- (1) H. Chen, C.E. Nanayakkara, V.H. Grassian, *Chem. Rev.*, 2012, 112, 5919-5948.
- (2) C. Chen, W. Ma, J. Zhao, *Chem. Soc. Rev.*, 2010, 39, 4206-4219.
- (3) L. Ye, Y. Su, X. Jin, H. Xie, C. Zhang, *Environ. Sci.: Nano.*, 2014, 1, 90-112.
- (4) A. Kubacka, M. Fernández-García, G. Colón, *Chem. Rev.*, 2012, 112, 1555-1614.
- (5) N. Serpone, A.V. Emeline, *J. Phys. Chem. Lett.*, 2012, 3, 673-677.
- (6) X. Chen, S. Shen, L. Guo, S.S. Mao, *Chem. Rev.*, 2010, 110, 6503-6570.
- (7) J. Mao, L. Ye, K. Li, X. Zhang, J. Liu, T. Peng, L. Zan, *Appl. Catal. B: Environ.*, 2014, 144, 855-862.
- (8) P. Wang, B. Huang, X. Qin, X. Zhang, Y. Dai, J. Wei, M.H. Whangbo, *Angew. Chem. Int. Ed.*, 2008, 47, 7931-7933.
- (9) C. An, S. Peng, Y. Sun, *Adv. Mater.*, 2010, 22, 2570-2574.
- (10) P. Wang, B. Huang, X. Zhang, X. Qin, H. Jin, Y. Dai, Z. Wang, J. Wei, J. Zhan, S. Wang, J. Wang, M. H. Whangbo, *Chem. Eur. J.*, 2009, 15, 1821-1824.
- (11) Z. Yi, J. Ye, N. Kikugawa, T. Kako, S. Ouyang, H. Stuart-Williams, H. Yang, J. Cao, W. Luo, Z. Li, Y. Liu, R.L. Withers, *Nat. Mater.*, 2010, 9, 559 -564.
- (12) Y. Bi, H. Hu, S. Ouyang, Z. Jiao, G. Lu, J. Ye, *Chem. Eur. J.*, 2012, 18, 14272-14275.
- (13) X. Wang, K. Maeda, A. Thomas, K. Takanabe, G. Xin, J.M. Carlsson, K. Domen, M.A. Antonietti, *Nat. Mater.*, 2009, 8, 76-80.
- (14) G. Liu, P. Niu, C. Sun, S.C. Smith, Z. Chen, G.Q. Lu, H.M. Cheng, *J. Am. Chem. Soc.*, 2010, 132, 11642-11648.
- (15) F. Wang, W.K.H. Ng, J. C. Yu, H. Zhu, C. Li, L. Zhang, Z. Liu, Q. Li, *Appl. Catal. B: Environ.*, 2012, 111-112, 409-414.
- (16) G. Liu, P. Niu, L. Yin, H.M. Cheng, *J. Am. Chem. Soc.*, 2012, 134, 9070-9073.
- (17) H. Cheng, B. Huang, Y. Dai, *Nanoscale*, 2014, 6, 2009-2026.
- (18) X. Zhang, Z. Ai, F. Fia, L. Zhang, *J. Phys. Chem. C.*, 2008, 112, 747-753.

- (19) K.L. Zhang, C.M. Liu, F.Q. Huang, C. Zheng, W.D. Wang, *Appl. Catal. B: Environ.*, 2006, 68, 125-129.
- (20) J. Jiang, K. Zhao, X. Xiao, L. Zhang, *J. Am. Chem. Soc.*, 2012, 134, 4473-4476.
- (21) L. Ye, J. Liu, C. Gong, L. Tian, T. Peng, L. Zan, *ACS Catal.*, 2012, 2, 1677-1683
- (22) L. Ye, J. Liu, Z. Jiang, T. Peng, L. Zan, *Appl. Catal. B: Environ.*, 2013, 142-143, 1-7.
- (23) L. Ye, J. Chen, L. Tian, J. Liu, T. Peng, K. Deng, L. Zan, *Appl. Catal. B: Environ.*, 2013, 130-131, 1-7.
- (24) J. Shang, W. Hao, X. Lv, T. Wang, X. Wang, Y. Du, S. Dou, T. Xie, D. Wang, J. Wang, *ACS Catal.*, 2014, 4, 954-961.
- (25) S. Sun, W. Wang, L. Zhang, L. Zhou, W. Yin, M. Shang, *Environ. Sci. Technol.*, 2009, 43, 2005-2010.
- (26) J. Wang, Y. Yu, L. Zhang, *Appl. Catal. B: Environ.*, 2013, 136-137, 112-121.
- (27) H.G. Yang, C.H. Sun, S.Z. Qiao, J. Zou, G. Liu, S.C. Smith, H.M. Cheng, G.Q. Lu, *Nature*, 2008, 453, 638-641.
- (28) L. Ye, J. Mao, J. Liu, Z. Jiang, T. Peng, L. Zan, *J. Mater. Chem. A*, 2013, 1, 10532-10537.
- (29) W.C. Huang, L.M. Lyu, Y.C. Yang, M.H. Huang, *J. Am. Chem. Soc.*, 2012, 134, 1261-1267.
- (30) H. Wang, J. Yang, X. Li, H. Zhang, J. Li, L. Guo, *Small*, 2012, 8, 2802-2806
- (31) Y. Bi, S. Ouyang, N. Umezawa, J. Cao, J. Ye, *J. Am. Chem. Soc.*, 2011, 133, 6490-6492.
- (32) D. Wang, H. Jiang, X. Zong, Q. Xu, Y. Ma, G. Li, C. Li, *Chem. Eur. J.*, 2011, 17, 1275-1282.
- (33) G. Kresse, J. Hafner, *J. Phys. Rev. B.*, 1993, 47, 558-561.
- (34) G. Kresse, J. Furthemüller, *J. Phys. Rev. B.*, 1996, 54, 11169-11186.
- (35) J.P. Perdew, K. Burke, M. Ernzerhof, *Phys. Rev. Lett.*, 1996, 77, 3865-3868.
- (36) P.E. Blöchl, *Phys. Rev. B.*, 1994, 50, 17953-17979.
- (37) G. Kresse, D. Joubert, *Phys. Rev. B.*, 1999, 59, 1758-1775.
- (38) R. Zhang, Y. Dai, Z. Lou, Z. Li, Z. Wang, Y. Yang, X. Qin, X. Zhang, B. Huang, *CrystEngComm*, 2014, 16, 4931-4934.
- (39) W. Wang, B. Huang, X. Ma, Z. Wang, X. Qin, X. Zhang, Y. Dai, M. H. Whangbo, *Chem. Eur. J.*, 19: 14777-14780.

---

## Caption

**Fig. 1.** XRD patterns of Bi<sub>5</sub>O<sub>7</sub>I rods and Bi<sub>5</sub>O<sub>7</sub>I sheets.

**Fig. 2.** FESEM images of Bi<sub>5</sub>O<sub>7</sub>I sheets (a) and Bi<sub>5</sub>O<sub>7</sub>I rods (d); SAED patterns of Bi<sub>5</sub>O<sub>7</sub>I sheets (b) and Bi<sub>5</sub>O<sub>7</sub>I rods (e); and HRTEM images and the corresponding FFT patterns (the inset picture) of Bi<sub>5</sub>O<sub>7</sub>I sheets (c) and Bi<sub>5</sub>O<sub>7</sub>I rods (f).

**Fig. 3.** UV-vis diffuse reflectance spectra and the plots of  $(ah\nu)^{1/2}$  vs. photon energy ( $h\nu$ ) of Bi<sub>5</sub>O<sub>7</sub>I sheets and Bi<sub>5</sub>O<sub>7</sub>I rods.

**Fig. 4.** The PCD percentage of RhB (a) and MO (b) under Xe lamp irradiation.

**Fig. 5.** PL spectra of Bi<sub>5</sub>O<sub>7</sub>I sheets and Bi<sub>5</sub>O<sub>7</sub>I rods with the excitation wavelength at 320 nm.

**Fig. 6.** Total DOS and partial DOS of Bi<sub>5</sub>O<sub>7</sub>I: (a) {001} facet, and (b) {100} facet.

**Fig. 7.** Trapping experiment of active species during the photocatalytic reaction with Bi<sub>5</sub>O<sub>7</sub>I rods.

**Scheme 1.** Photocatalytic mechanism scheme of the shape-dependent photocatalytic activity of Bi<sub>5</sub>O<sub>7</sub>I.

**Scheme 2.** The transfer process of photoinduced holes between {001} and {100} facets.

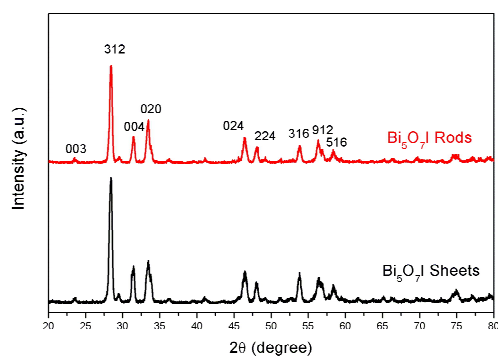


**Fig. 1.** XRD patterns of  $\text{Bi}_5\text{O}_7\text{I}$  rods and  $\text{Bi}_5\text{O}_7\text{I}$  sheets.

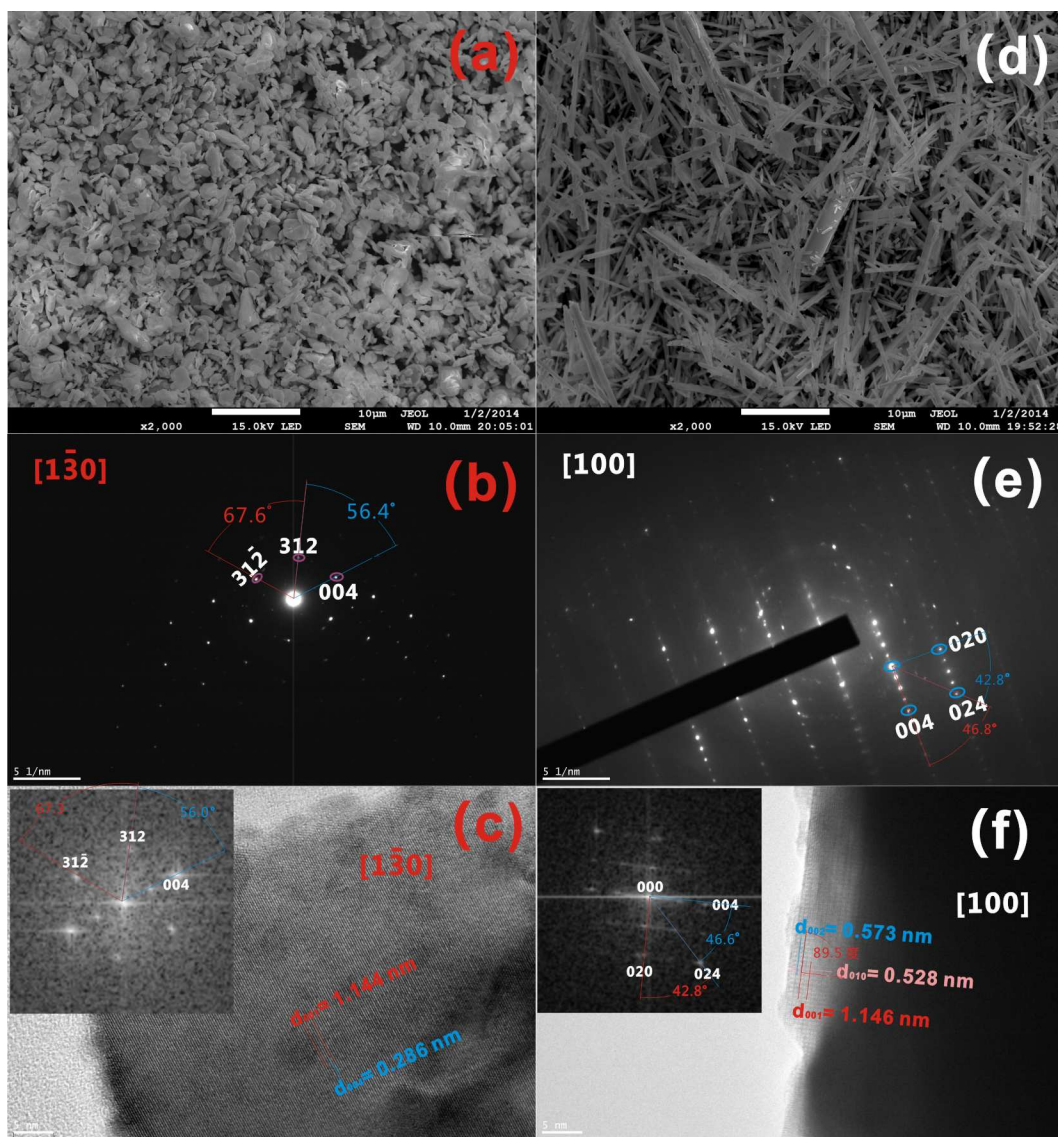


**Fig. 2.** FESEM images of  $\text{Bi}_5\text{O}_7\text{I}$  sheets (a) and  $\text{Bi}_5\text{O}_7\text{I}$  rods (d); SAED patterns of  $\text{Bi}_5\text{O}_7\text{I}$  sheets (b) and  $\text{Bi}_5\text{O}_7\text{I}$  rods (e); and HRTEM images and the corresponding FFT patterns (the inset picture) of  $\text{Bi}_5\text{O}_7\text{I}$  sheets (c) and  $\text{Bi}_5\text{O}_7\text{I}$  rods (f).

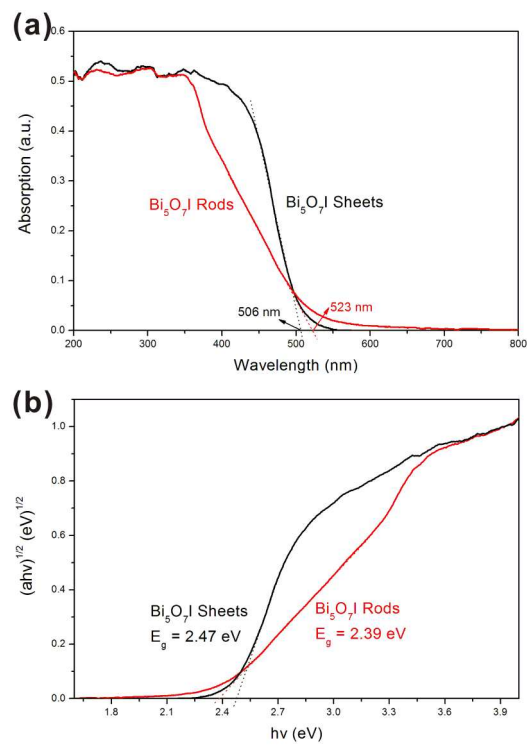


**Fig. 3.** UV-vis diffuse reflectance spectra and the plots of  $(\alpha h\nu)^{1/2}$  vs. photon energy ( $h\nu$ ) of  $\text{Bi}_5\text{O}_7\text{I}$  sheets and  $\text{Bi}_5\text{O}_7\text{I}$  rods.

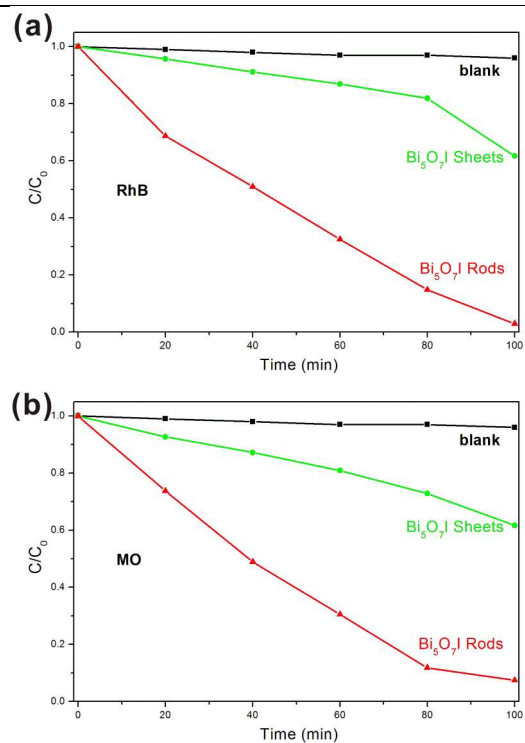


**Fig. 4.** The PCD percentage of RhB (a) and MO (b) under Xe lamp irradiation.

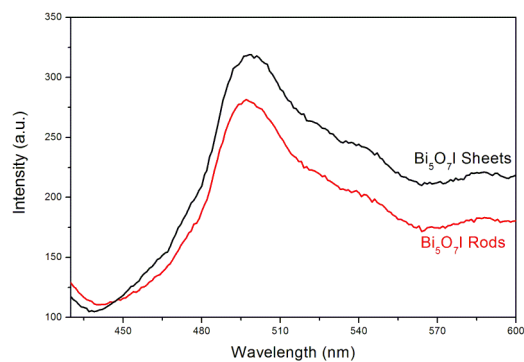


**Fig. 5.** PL spectra of Bi<sub>5</sub>O<sub>7</sub>I sheets and Bi<sub>5</sub>O<sub>7</sub>I rods with the excitation wavelength at 320 nm.

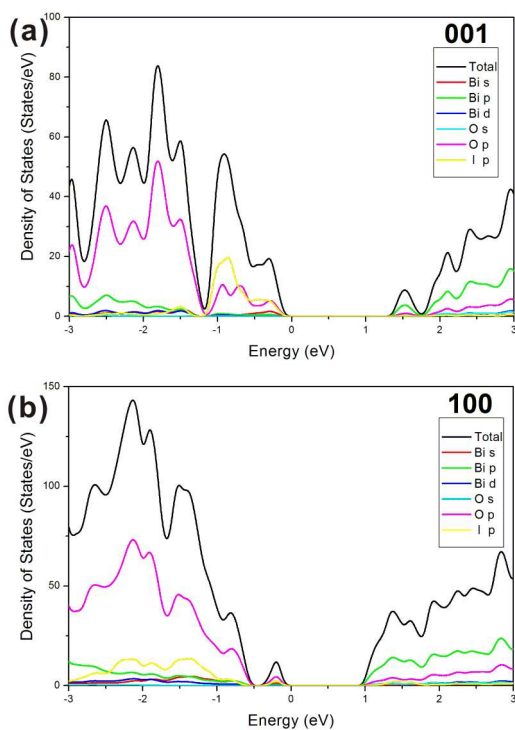


**Fig. 6.** Total DOS and partial DOS of Bi<sub>5</sub>O<sub>7</sub>I: (a) {001} facet, and (b) {100} facet.

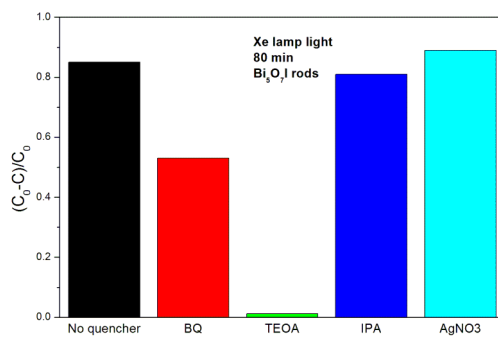
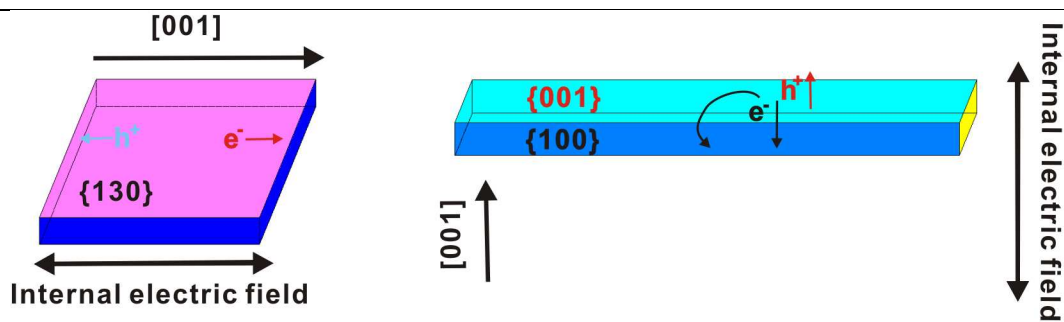
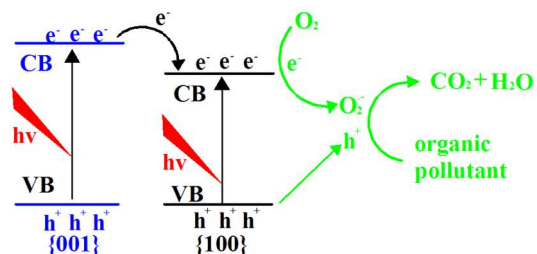


**Fig. 7.** Trapping experiment of active species during the photocatalytic reaction with Bi<sub>5</sub>O<sub>7</sub>I rods.

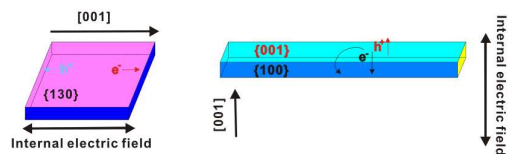


**Scheme 1.** Photocatalytic mechanism scheme of the shape-dependent photocatalytic activity of  $\text{Bi}_5\text{O}_7\text{I}$ .



**Scheme 2.** The transfer process of photoinduced holes between  $\{001\}$  and  $\{100\}$  facets.

## TOC



The shape-dependent photocatalytic activity of  $\text{Bi}_5\text{O}_7\text{I}$  is caused by facets synergetic and internal electric field effects.